Autonomously-triggered microfluidic cooling using thermo-responsive hydrogels

Abhishek K. Agarwal,†[a] Liang Dong,[a] David J. Beebe[b] and Hongrui Jiang*[a]

Received 13th July 2006, Accepted 11th December 2006
First published as an Advance Article on the web 3rd January 2007
DOI: 10.1039/b617767k

We present autonomously-triggered on-chip microfluidic cooling devices that utilize thermo-responsive hydrogels to adapt to local environmental temperatures. An external rotating magnetic stirrer couples with an *in situ* fabricated nickel impeller in these centrifugal-based microfluidic cooling devices to recirculate cooler water. Temperature-responsive hydrogels, which exhibit volumetric expansion and contraction, are integrated at the axle of the impeller. In this design, the hydrogels behave similar to an automotive clutch, to autonomously control the impeller's rotation as a function of the local environmental temperature. Therefore, the hydrogels act as both sensors and actuators and help take away the necessity for additional temperature sensing, feedback, and/or control units here. Cooling devices capable of on-chip thermal management at multiple predetermined onset operation points are realized by changes to the composition of hydrogel to alter its lowest critical solution temperature (LCST). Furthermore, the effect of magnetic stirrer frequency on the fluid cooling and flowrates for different two-blade nickel impeller designs are presented.

Introduction

On-chip thermal management is an area of research in emerging lab-on-a-chip systems and biological microfluidics that still needs further development, especially for microscale systems.[1,2] Several mechanisms currently exist for provision of heating, including Peltier devices[1,3,4] and thin-film heaters;[5–7] however, cooling, which can be facilitated by technologies such as air-cycling[8,9] and pumps,[10] generally requires feedback sensors and control systems, and may not be easily scaled down and/or integrated into devices at the microscale.

Here, we report on autonomously-triggered on-chip microfluidic cooling devices that utilize thermo-responsive hydrogels[11–14] and do not require additional temperature sensing and feedback electronics. Temperature-responsive hydrogels inherently react to local environmental temperatures to enable autonomous microfluidic cooling. The centrifugal-based cooling mechanism[15] combines an electroformed nickel (Ni) impeller with polymer-based microfluidics and a temperature-responsive hydrogel. Here, an external rotating magnetic stirrer drives the Ni impeller to recirculate cooler water. The temperature-responsive hydrogel ring is photopatterned around the center axis of the Ni impeller, and autonomously responds by expanding and contracting in volume when exposed to low and high temperatures, respectively. This clutching mechanism controls the on/off rotational status of the Ni impeller and helps facilitate the device to autonomously adapt to local environmental temperatures, with the hydrogel acting as both the sensor and actuator.[16] This unique characteristic of being self-adaptive to local environmental temperatures enables the cooling devices to realize autonomous control. Two onset operation temperature regimes are demonstrated by chemically changing the temperature-responsive hydrogel's lowest critical solution temperature (LCST)[17,18]—the temperature regime in which the hydrogel exhibits the largest change in volume. Furthermore, studies are presented on how varying magnetic stirrer frequencies affect the average fluid cooling and flowrates for different two-blade Ni impeller geometries.

[a]*Department of Electrical and Computer Engineering, University of Wisconsin-Madison, 1415 Engineering Drive, Madison, WI 53706, USA. E-mail: hongrui@engr.wisc.edu; Fax: 1-608-262-1267; Tel: 1-608-265-9418*
[b]*Department of Biomedical Engineering, University of Wisconsin-Madison, 1550 Engineering Drive, Madison, WI 53706, USA*
† Present address: Department of Biomedical Engineering, Northwestern University, 2145 Sheridan Road, Evanston, IL 60208, USA.

Materials and methods

Chemical and hardware materials

Isobornyl acrylate (IBA) is used as received from Surface Specialties UCB (Smyma, GA, USA). Tetraethylene glycol dimethacrylate (TeGDMA, 90%), 2,2-dimethoxy-2-phenylacetophenone (DMPA, 99%), 3-(methacryloylamino)propyl trimethylammonium chloride (MAPTAC, 50 wt.% in water solution, 600 ppm inhibitor), and fluorescein sodium salt ($\lambda_{excitation}$ = 460 nm; $\lambda_{emission}$ = 515 nm) are from Sigma-Aldrich (St. Louis, MO, USA). *N*-Isopropylacrylamide (NIPAAm; recrystallized once), *N*,*N*′-methylenebisacrylamide (NMBA, electrophoresis grade), and dimethyl sulfoxide (DMSO, 99.6 + %) are from Acros Organics (Morris Plains, NJ, USA).

A triple output DC power supply (model E3631A) is from Agilent Tech. (Palo Alto, CA, USA). A digital color camera with fluorescence imaging capability (model DFC300 FX) is from Leica Microsystems, Ltd. (Allendale, NJ, USA). A stereo

microscope with a mercury lamp fluorescence module (model SZX12) is from Olympus America (Center Valley, PA, USA). The Kapton heater (model HK5537R7.8L12A, diameter, ϕ_{heater} = 12.7 mm) is from Minco (Minneapolis, MN, USA). A thermally-conductive double-side adhesive tape (# 9885) is from 3M (St. Paul, MN, USA). Type-K thermocouples (model 5SC-TT-K-40-36) and a multilogger thermometer with RS232-C (model HH506RA) are obtained from Omega Engr. (Stamford, CT, USA). Polycarbonate cartridges with adhesive gaskets around the edge (125 and 250 μm thick) are from Grace Bio-Labs (Bend, OR, USA). The external rotating magnetic stirrer (model 84) is from Cole Parmer (Vernon Hills, IL, USA). An EXFO Acticure A4000 (EXFO Life Sciences, Mississauga, ON, Canada) spot-cure ultraviolet (UV) light source is used to photopattern the photosensitive polymers. High resolution (3600 dpi) film photomasks from Silverline Studio (Madison, WI, USA) are used to transfer the patterns to the polymers.

Precursor solutions

Three UV-photosensitive precursor solutions are prepared by mixing: (1) poly(IBA)—a non-responsive precursor solution consisting of 1.9 mL IBA (monomer), 0.1 g TeGDMA (crosslinker), and 0.06 g DMPA (photoinitiator). It is used to form the microfluidic structures (*e.g.*, microfluidic channels and posts). (2) NIPAAm 1—a precursor solution consisting of 0.0385 g DMPA, 0.545 g NIPAAm (monomer), 0.031 g NMBA (crosslinker), 0.75 mL DMSO (solvent), and 0.25 mL deionized (DI) water (solvent). (3) NIPAAm 2—a precursor solution consisting of the same constituents as NIPAAm 1, with an additional 0.0531 mL MAPTAC (co-monomer). The poly(NIPAAm) hydrogel precursor solutions are responsive to local environmental temperatures—the hydrogel expands in volume at low local temperatures and contracts at high temperatures.[11–14] It has been shown that incorporating hydrophobic (hydrophilic) co-monomers leads to a lower (higher) LCST,[17] *i.e.*, a shift in the temperature response and change in the swelling behavior. Incorporation of MAPTAC, an ionizable co-monomer into the NIPAAm hydrogel network has shown increases in the hydrogel's LCST.[18] The mole percentages of MAPTAC are defined with respect to the amount of NIPAAm, which pre-programs the lowest critical solution temperature (LCST), *i.e.*, the onset operation temperature of the cooling pump.

Fabrication of cooling device

The two-layer microfluidic cooling device was fabricated using liquid-phase photopolymerization (LP^3)[19] and Ni electroforming.[16,20] Merging the two technologies leverages several advantages that have been previously used to realize a variety of programmable autonomous microfluidic components.[16,20] A step-and-repeat LP^3 process helps realize *in situ* fabrication of polymer structures, which can also serve as die-cast molds for Ni electroforming.[16,20] The fabrication process is briefly described here for the two-layer microfluidic cooling device. This process leverages techniques and procedures that have been reported in detail elsewhere.[20]

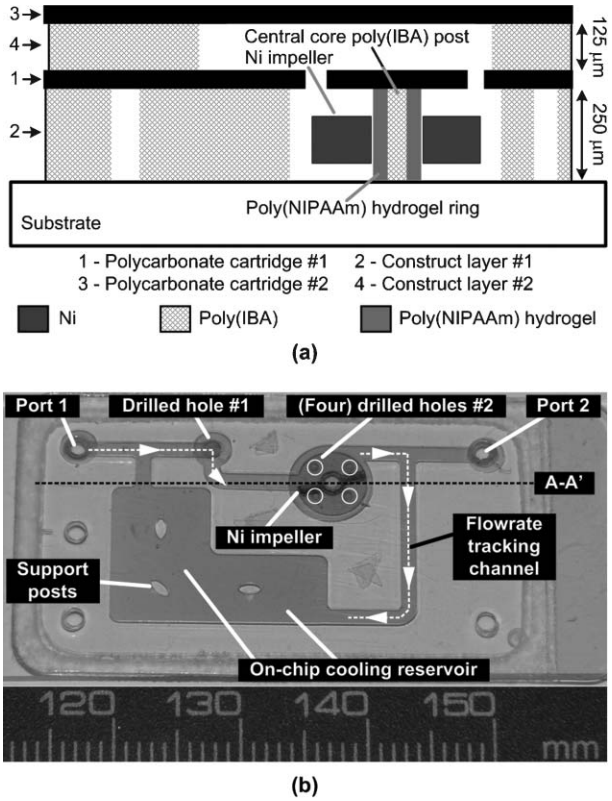

Fig. 1 An autonomously-triggered on-chip microfluidic cooling device. The device is driven by an external rotating magnetic stirrer. (a) Cross-section of the two-layer device at A–A′ in (b). Holes drilled in cartridge #1 allow fluid transfer between the two polymer construct layers. Liquid-phase photopolymerization is used to photopattern the poly(IBA) microchannels and posts, and poly(NIPAAm) hydrogel ring. This temperature-responsive hydrogel ring acts similar to an automotive clutch by expanding and contracting in volume, and subsequently controlling the rotational status of the Ni impeller. (b) Photograph of the final device. The dashed white line and arrows show the partial pathway of the fluid as it is pumped and recirculated through the microchannels.

Fig. 1(a) shows a cross-sectional diagram of the two-layer microfluidic cooling device at A–A′ shown in Fig. 1(b). A poly(IBA) mold which defines the shape of the Ni impeller was photopatterned on a glass slide substrate previously coated with metal seed layers (Ti/Cu/Ti). Cu was used as the seed layer for Ni electroforming. After the Ni impeller was electroformed, the poly(IBA) mold was removed after soaking in a 3 : 1 methanol : acetone solution for 4–5 h. The underlying exposed metal seed layers were removed using wet-etching. Five holes (ϕ = 1.12 mm (#1) and 0.49 mm (#2)) were drilled in a 250 μm thick polycarbonate cartridge #1 (Fig. 1(a)). The cartridge was adhered to the glass slide substrate, followed by the step-and-repeat LP^3 patterning of: central core poly(IBA) post; poly(NIPAAm) hydrogel ring; and poly(IBA) microchannels and cooling reservoir. They were formed in construct layer #1. The Ni impeller was released from the glass slide substrate by wet-etching the underlying metal seed layers. Next, construct layer #1 (poly(IBA) microchannel network photodefined inside the cartridge) was filled with a glycerin–water liquid sacrificial layer to prevent the backflow of the

poly(IBA) precursor solution through holes and ports #1 and #2 introduced in the next step. Next, the 125 μm thick polycarbonate cartridge (#2) was adhered on top of first cartridge and the poly(IBA) microchannel in construct layer #2 was photopatterned similarly, thereby connecting the two sets of holes. All photopatterned microchannels were 1.25 mm wide. Fig. 1(b) shows a photograph of the final device.

Results

Three sets of experiments were performed to evaluate the two-layer microfluidic cooling devices. The first experiment observed the autonomous functionality in multiple temperature regimes, *i.e.*, on/off status of the pumping when local temperatures were varied above and below the hydrogel's respective LCST (onset operation temperature). Two distinct temperature operation regimes were realized and demonstrated by chemically changing the hydrogel's LCST. The second experiment determined the effect of different stirrer frequencies on the average fluid cooling for four different Ni impeller blade geometries. The third experiment determined the effect of different stirrer frequencies on the average flowrates achieved by the same Ni impeller blades. For the latter two experiments, the devices did not have a temperature-sensitive hydrogel integrated into the axle, since only the performance of the impeller was being presented.

Cooling device operation

Here, the Ni impeller in the autonomous microfluidic cooling device coupled with an external rotating magnetic stirrer, and recirculated water (centrifugal-based pumping). Using thermal conductive double-sided tape, a Kapton heater was adhered to the underside of the device (directly beneath the impeller) to mimic the local heat source. Water was recirculated from the cooling reservoir into the microchannels in construct layer #1 (see Fig. 1). It flowed through hole #1 to construct layer #2; then, it flowed inside this microchannel and fell down onto the rotating Ni impeller *via* holes #2, and flowed back into the construct layer #1 microchannel. The cooling reservoir was kept away from the local heater (Fig. 2(a)), and thus maintained a lower cooled temperature. The on/off status of the cooling device was controlled autonomously by the temperature-responsive hydrogel (described next).

Autonomous functionality in response to local environmental temperatures

Experiments were performed to evaluate the autonomous functionality of two autonomous microfluidic cooling pumps with poly(NIPAAm) hydrogels (NIPAAm 1 and 2) that differed in their onset operation temperature. The Kapton heater was driven by a DC power supply to provide local heating. A thermocouple, connected to a multilogger thermometer, was used to monitor the local fluid temperatures inside the microchannel at the T-junction shown in Fig. 2. The thermometer, which was connected to a portable laptop *via* a RS232-C port, recorded the data every 10 s. See Fig. 2 for the experimental setup. The photopatterned poly(NIPAAm) hydrogel ring contracted (see left inset photo in Fig. 2; approximate area of hydrogel was 1.04 mm^2) and expanded (see right inset photo in Fig. 2; approximate area of hydrogel was 1.54 mm^2) in volume when exposed to high and low local temperatures, respectively. These volumetric shifts enabled the responsive hydrogel to behave similar to an automotive clutch, thereby controlling the on (left inset photo in Fig. 2) and off (right inset photo in Fig. 2) rotational status of the Ni impeller in the presence of the constant external rotating magnetic stirrer. Experiments were performed under the presence of a constant external rotating magnetic stirrer with a rotational frequency (f) of 12.5 Hz. To observe the autonomous pumping mechanism, the heater temperature was gradually increased from room temperature to a higher temperature until visual observations showed the Ni impeller rotating, and recirculating cooler water. The onset of rotation was recorded as the 'pumping on' temperature. The heater was subsequently turned off to lower the local temperature through heat dissipation. The termination of rotation was recorded as the 'pumping off' temperature. This heating and cooling cycle was repeated for five cycles for repeatability. The experimental conditions, and resulting onset and termination temperatures for both poly(NIPAAm) responsive hydrogels are shown in Table 1. Visual observations showed that NIPAAm 1 and

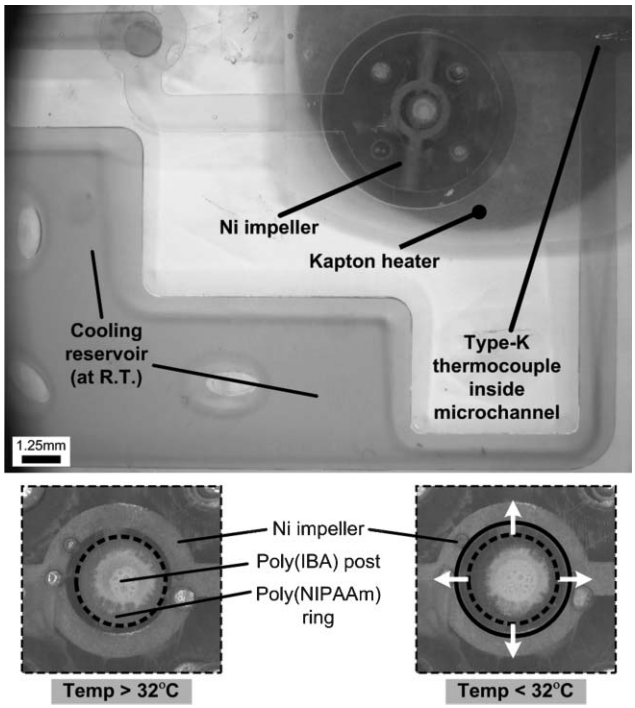

Fig. 2 Experimental setup for the autonomously-triggered on-chip microfluidic cooling pump. The device is driven by an external rotating magnetic stirrer. A Kapton heater adhered to the underside of the device simulates local heating. A type-K thermocouple inserted inside the microchannel is used to monitor the local fluid temperature. The on-chip cooling reservoir is at room temperature. Here, when local temperatures are above 32 °C, the hydrogel contracts; the Ni impeller rotates, and pumps and recirculates cooler water (see left inset photo; the dashed black circle shows the contracted hydrogel boundary). When local temperatures drop below 32 °C, the hydrogel expands (see right inset photo; expansion occurs from dashed black circle to solid circle). Hence, the Ni impeller stops rotating.

Table 1 Observations of the autonomous pumping/cooling functionality (on/off) of two autonomous cooling pumps with different onset operation temperatures in the presence of a constant external rotating magnetic stirrer

		NIPAAm **1**	NIPAAm **2**
Experimental setup	Room temperature/°C	24.5 ± 0.3	25.0 ± 0.3
	Heater setpoint/°C	40.0	75.0
	Cooling reservoir temperature/°C	24.3	24.5
	Magnetic stirrer frequency/Hz	12.5	12.5
Observed autonomous functionality	Pumping on/°C	32.5 ± 0.3	60.4 ± 0.5
	Pumping off/°C	27.6 ± 0.2	55.5 ± 0.6
Device characteristics	LCST/°C	~32	~60

NIPAAm 2 began to recirculate cooler water at 32.5 ± 0.3 °C and 60.4 ± 0.5 °C, respectively; both devices stopped recirculating cooler water at 27.6 ± 0.2 °C and 55.5 ± 0.6 °C, respectively.

By modifying the quantity of MAPTAC added to the poly(NIPAAm) hydrogel network, it is feasible to design autonomously-triggered on-chip microfluidic cooling devices suitable for a variety of applications and processes that necessitate specific temperature regulation. Furthermore, by utilizing the step-and-repeat LP^3 process, integrating multiple poly(NIPAAm) hydrogels with different LCSTs into a single device can also be realized with relative ease.

Fluid cooling

Experiments were conducted to determine the effect of magnetic stirrer frequency on the average fluid cooling for four different two-blade Ni impeller geometries that varied in length, width, and thickness, respectively: 'A' −2.0, 0.40 and 0.10 ± 0.013 mm; 'B' −2.0, 0.80 and 0.10 ± 0.013 mm; 'C' −3.0, 0.40 and 0.10 ± 0.013 mm; 'D' −2.0, 0.40 and 0.20 ± 0.007 mm. The small deviations in blade thickness resulted from the variations in the rate of Ni electroforming. The experimental setup was the same as previously mentioned for autonomous functionality and shown in Fig. 2. Four magnetic stirrer frequencies were studied −6, 12.5, 19, and 25 Hz. To simulate on-chip heating, a constant heat flux was inputted into the microfluidic cooling system by maintaining a constant DC power supply to the Kapton heater to realize a heater setpoint, H_s, equal to 50 ± 0.5 °C.

To determine the average fluid cooling and cooling rate associated with each device, the external rotating magnetic stirrer was turned on and off. When the stirrer was on, the cooling pump was activated and allowed to reach a stable low fluid temperature (T_f) from the recirculation of cooler water; when the stirrer was off, the cooling device ceased to operate, and the fluid temperature gradually returned to H_s. The magnetic stirrer was turned on/off for five cycles. The fluid cooling was defined as $\Delta T = H_s - T_f$; cooling rate was defined as average fluid cooling divided by the time taken to reach T_f. The inset data plot in Fig. 3 shows an example of local fluid temperature *vs.* time for device 'B' at f = 25 Hz. The microfluidic cooling device reached stable temperatures consistently, as shown by three of the five cyclical troughs and crescents. Here, device 'B' was able to realize an average fluid cooling (ΔT) and average fluid cooling rate of 6.6 ± 0.2 °C and 2.0 ± 0.4 °C min^{-1}, respectively.

Similar experiments were repeated with the other three devices ('A', 'C', and 'D') for the four different magnetic stirrer frequencies (Fig. 3, right-axis). Increasing the blade length ('A' and 'C') might cause an increase in the average fluid cooling (on average, by 0.1–1.8 °C across all four frequencies) since a longer impeller blade will be able to create larger centrifugal forces to recirculate the cooler fluid. Increasing the blade width ('A' *vs.* 'B') had minimal effect on the average fluid cooling (on average, by 0.2–0.7 °C). Impeller thickness ('A' *vs.* 'D') had no effect on the average fluid cooling here. Average fluid cooling rates were not generally impacted and similar performance was observed (not shown) for the Ni impeller lengths, widths, and thicknesses studied here.

An overall general observation shown by Fig. 3 is that as stirrer frequency increases, the cooling increases for each respective Ni impeller. It is believed that not only is thermal dispersion from the fabrication materials readily enabling fluid cooling, but the active distribution and movement of the liquid inside the circular pumping chamber (Fig. 1(b)) as a result of the rotating Ni impeller also assists in cooling.

Fluid flowrate

Experiments were conducted to determine the effect of magnetic stirrer frequency on the average flowrate for devices 'A'–'D'. The experimental setup was the same as previously mentioned for fluid cooling and cooling rates. For experimental continuity, a constant heat flux was inputted into the microfluidic cooling system by the Kapton heater to realize H_s equal to 50 ± 0.5 °C. The experiments on the four devices were done under the observation of a stereo microscope with a digital camera attached to its photoport. A 0.4 wt.% fluorescein sodium salt and water solution was used to track the fluid front *via* fluorescent imaging with the digital camera.

The microchannel network of a device was initially filled with DI water and subsequently, the device was positioned on the magnetic stirrer, previously stabilized at one of the four rotational frequencies (6, 12.5, 19, and 25 Hz). Once the impeller's rotation had stabilized for 180 s, a large drop (~100–300 μL) of the fluorescein : water solution was placed at 'port 1' (see Fig. 1(b)). The system was allowed to equilibrate for 60 s to ensure that the dye did not flow due to any pressure differences between 'port 1' and 'port 2' (Fig. 1). A disposable transfer pipette was used to suck out a small amount of fluid from 'port 2' such that the fluorescent dye was introduced into the construct layer #1 microchannel and reached hole #1. Next, the device's fluid recirculation took over and the fluorescent dye followed the path shown in Fig. 1(b) by the dashed white lines and arrows. Images of the dye front were acquired in the 'flowrate tracking channel' *via* the digital camera at preset time intervals ranging from 1–30 s.

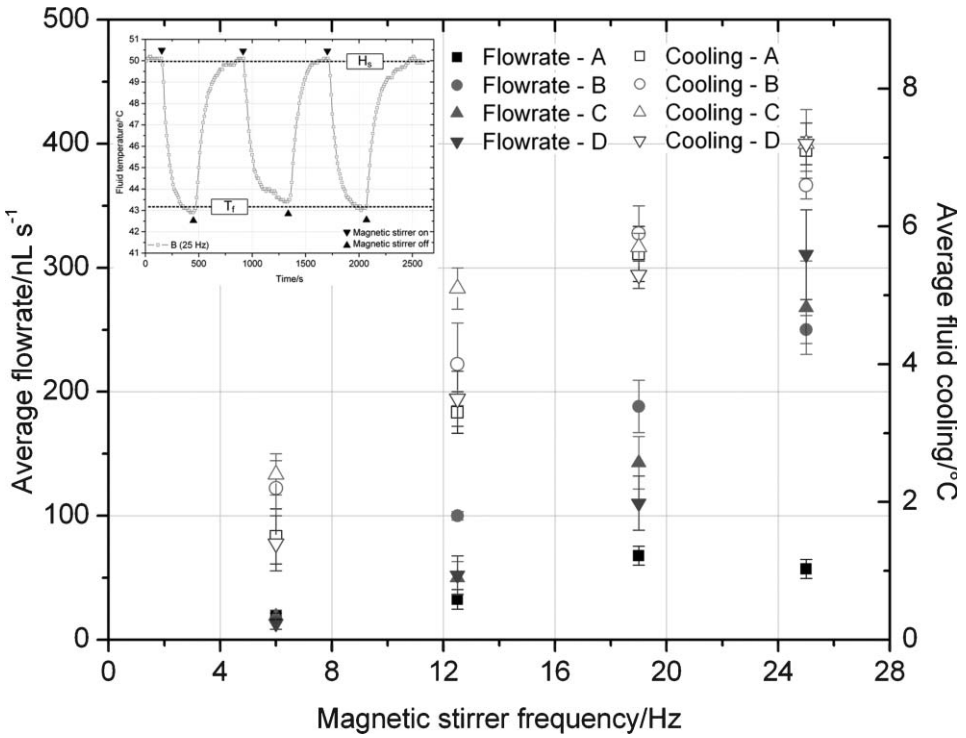

Fig. 3 Effect of magnetic stirrer frequency on the average flowrate (left axis; error bars, σ along flowrate tracking channel) and cooling ($\Delta T = H_s - T_f$, right axis; error bars, σ over five recurring cycles) for four different two-blade Ni impeller devices ('A'–'D') in the presence of a constant heat influx (H_s is 50 $\pm$ 0.5 °C). Impeller blade length, width, and thickness have an effect on achieved flowrates at high stirrer frequencies; however, the resulting higher flowrates do not correspond to higher average fluid cooling, *e.g.*, 'A' maintains high fluid cooling despite a low flowrate at f = 25 Hz. It is believed that the drop in flowrate for 'A' at f = 25 Hz is due to inefficient coupling of the impeller with the magnetic stirrer, *i.e.*, an operating threshold limit. The inset data plot shows an example of local fluid temperature *vs.* time for device 'B' at H_s. The external magnetic stirrer (here, set to 25 Hz) is turned on ('▼') and off ('▲') for five cycles (three shown here) to activate and deactivate the device's recirculation of cooler water from the on-chip reservoir. The microfluidic cooling device reaches low fluid temperatures (T_f) consistently, as shown by the three cyclical troughs. Here, device 'B' realizes an average fluid cooling (ΔT) and average fluid cooling rate of 6.6 $\pm$ 0.2 °C and 2.0 $\pm$ 0.4 °C min^{-1}, respectively.

NIH ImageJ ver. 1.32j software was used to observe nine separate positions of the dye front along the 'flowrate tracking channel' to determine the average fluid velocity. The average fluid flowrates were subsequently determined by multiplying the respective fluid velocity with the microchannel cross-sectional area (here, 1.25 $\times$ 0.25 mm).

Fig. 3 shows the effect of magnetic stirrer frequency on both the average flowrate (left-axis) and average cooling (ΔT, right axis). At 6 Hz, the impeller geometry had no impact on the average fluid flowrate; however, as the stirrer frequency increases, distinguished observations could be made about each impeller's respective flowrates. The flowrates exhibited by 'A' increased with f; however, at f = 25 Hz, visual observations showed the impeller was not rotating smoothly. It is believed that the impeller was unable to maintain sufficient coupling with the rotating magnetic stirrer at such a high stirrer frequency causing the flowrate to decrease by $\sim$10 nL s^{-1}, *i.e.*, the impeller's operating threshold limit. Increasing the blade width ('B'), length ('C'), and thickness ('D') resulted in higher average fluid flowrates at $f \geqslant$ 12.5 Hz with no loss of coupling observed. Device 'D' had a blade thickness (200 μm) that closely matched the height of the microfluidic channel (250 μm). Therefore, the thicker impeller may create more pressure gradients to facilitate high flowrates, especially at f = 25 Hz.

An interesting observation that can be made from Fig. 3 is that flowrate seems to have little effect on the fluid cooling. Further studies with accurate modeling and experiments may help provide greater insight into this behavior by investigating the relationship between fluid flow and heat dissipation. In addition to the design of the responsive hydrogel chemistry (*i.e.*, LCST), data on fluid cooling, cooling rate, and flowrate can be useful in the design of an autonomous microfluidic cooling device for applications requiring specific and precise temperature regulation parameters. Choosing an optimal Ni impeller blade will allow proper control of the achieved cooling, rate of cooling, and fluid flowrates.

Conclusion

We have demonstrated an autonomously-triggered on-chip microfluidic cooling device by integrating polymer and Ni microstructures using LP^3. It has the potential to be integrated and applied in applications where on-chip temperature control and regulation is necessary. The temperature-responsive hydrogels respond to the local environmental temperatures, and enable autonomous operation of the microfluidic cooling device *via* pumping and recirculation of cooler water. The Ni impeller in the device couples with an external rotating magnetic stirrer to drive the fluid recirculation mechanism.

We have also shown here that by changing the chemistry of the poly(NIPAAm) responsive hydrogel *via* the addition of an ionizable co-monomer, MAPTAC, it is feasible to change its respective LCST and subsequently, the operation temperature range (here, two are demonstrated: 27–32 °C and 55–60 °C) in which the microfluidic cooling device functions. The effect of the magnetic stirrer frequency on the average fluid cooling, and flowrate for four two-blade Ni impellers differing in blade length, width, and thickness was presented to enable future optimization of the microfluidic cooling devices. These aforementioned characteristics can be optimally designed to fit microfluidic applications where on-chip multi-temperature management is necessary. Although devices presented here have relatively slow response times and cooling response rates, faster hydrogel response times (*e.g.*, sub-second[21]) could be achieved by reducing the dimensions of the hydrogel structures. Optimization of the device (*e.g.*, Ni impeller, microchannel geometry, hole diameters and position) may help realize faster cooling. Thus, these devices might eventually be applied for on-chip cooling, such as in PCR and cell culture.[2,22]

Further studies remain to be done. It would be helpful to observe the fluid patterns and mechanics created by the different impeller geometries to better gauge their respective abilities to recirculate fluid. More accurate modeling of the fluid cooling (*i.e.*, consideration of fluid convection, thermal radiation, and heat exchange) will enable better understanding of the cooling behavior exhibited by these cooling devices and help improve their performance. Also, here, an external rotating magnetic stirrer is used to drive the device, however, it is feasible to integrate an on-chip local actuator.[23] Additionally, different responsive hydrogels can lead to autonomous operation of the microfluidic devices to different environmental parameters.[12,13]

Acknowledgements

This research was partly supported by the Wisconsin Alumni Research Foundation and partly by the U.S. Department of Homeland Security (DHS) (grant #N-00014-04-1-0659), through a grant awarded to the National Center for Food Protection and Defense (NCFPD) at the University of Minnesota. The authors would like to thank the Wisconsin Center for Applied Microelectronics (WCAM) facility at the University of Wisconsin-Madison for cleanroom processing. The authors acknowledge Sudheer Sridharamurthy (University of Wisconsin-Madison) for technical assistance, and Dr Heiko J. van der Linden (University of Groningen, Netherlands) and Vinay Abhyankar (University of Wisconsin-Madison) for technical discussions.

References

1 G. Maltezos, M. Johnston and A. Scherer, *Appl. Phys. Lett.*, 2005, **87**, 154105.
2 D. J. Sadler, R. Changrani, P. Roberts, C.-F. Chou and F. Zenhausern, *IEEE Trans. Compon. Packag. Technol.*, 2003, **26**, 309–316.
3 P. Wilding, M. A. Shoffner, J. Cheng, G. Hvichia and L. J. Kricka, *Clin. Chem.*, 1995, **41**, 1367–1368.
4 A. T. Woolley, D. Hadley, P. Landre, A. J. deMello, R. A. Mathies and M. A. Northrup, *Anal. Chem.*, 1996, **68**, 4081–4086.
5 Y. Ueno, T. Horiuchi, T. Morimoto and O. Niwa, *Anal. Chem.*, 2001, **73**, 4688–4693.
6 E. T. Lagally, P. C. Simpson and R. A. Mathies, *Sens. Actuators, B*, 2000, **63**, 138–146.
7 Q. Xiang, B. Xu, R. Fu and D. Li, *Biomed. Microdevices*, 2005, **7**, 273–279.
8 C. T. Wittwer, G. C. Fillmore and D. J. Garling, *Anal. Biochem.*, 1990, **186**, 328–331.
9 C. T. Wittwer and D. J. Garling, *BioTechniques*, 1991, **10**, 76–83.
10 J. Darabi, M. M. Ohadi and D. DeVoe, *J. Microelectromech. Syst.*, 2001, **10**, 98–106.
11 M. Shibayama, S. Mizutani and S. Nomura, *Macromolecules*, 1996, **29**, 2019–2024.
12 D. J. Beebe, J. S. Moore, J. M. Bauer, Q. Yu, R. H. Liu, C. Devadoss and B.-H. Jo, *Nature*, 2000, **404**, 588–590.
13 Y. Osada, J. P. Gong and Y. Tanaka, *J. Macromol. Sci., Polym. Rev.*, 2004, **C44**, 87–112.
14 L. Dong, A. K. Agarwal, D. J. Beebe and H. Jiang, *Nature*, 2006, **442**, 551–554.
15 A. K. Agarwal, S. S. Sridharamurthy, D. J. Beebe and H. Jiang, *Proc. 13th Intl. Conf. on Solid-state Sensors, Actuators, and Microsystems*, Seoul, South Korea, 2005, IEEE, Piscataway, NJ, USA, 2005, pp. 364–367.
16 A. K. Agarwal, S. S. Sridharamurthy, D. J. Beebe and H. Jiang, *J. Microelectromech. Syst.*, 2005, **14**, 1409–1421.
17 H. Feil, Y. H. Bae, F. J. Jan and S. W. Kim, *Macromolecules*, 1993, **26**, 2496–2500.
18 H. J. van der Linden, W. Othuis and P. Bergveld, *Lab Chip*, 2004, **4**, 619–624.
19 D. J. Beebe, J. Moore, Q. Yu, R. H. Liu, M. L. Kraft, B.-H. Jo and C. Devadoss, *Proc. Natl. Acad. Sci. U. S. A.*, 2000, **97**, 13488–13493.
20 A. K. Agarwal, D. J. Beebe and H. Jiang, *J. Micromech. Microeng.*, 2006, **16**, 332–340.
21 A. Richter, D. Kuckling, S. Howitz, T. Gehring and K.-F. Arndt, *J. Microelectromech. Syst.*, 2003, **12**, 748–753.
22 J. Liu, M. Enzelberger and S. Quake, *Electrophoresis*, 2002, **23**, 1531–1536.
23 M. Barbic, J. J. Mock, A. P. Gray and S. Schultz, *Appl. Phys. Lett.*, 2001, **79**, 1399–1401.